EXTENDING THE UHPC PI-GIRDER CONCEPT: OPTIMIZED CROSS-SECTIONS FOR SPAN UP TO 135 FEET

Gang Zhang, PhD, PE, PSI Inc., Turner-Fairbank Highway Research Center, McLean, VA
Benjamin A. Graybeal, PhD, PE, FHWA, Turner-Fairbank Highway Research Center, McLean, VA

ABSTRACT

As a class of advanced cementitious composite materials, ultra-high performance concrete (UHPC) presents opportunities to optimize the structural configuration of highway bridge superstructure systems. Past research and deployment efforts have demonstrated that the pi-girder concept is viable from the structural design, fabrication, and construction standpoints. This computational investigation focused on developing a series of finite element optimized sections of pi-girders to effectively utilize the superior mechanical properties of UHPC over longer span lengths. The research was performed using the previously calibrated concrete damaged plasticity model to represent the elastic and plastic response of the UHPC. The new cross-sections were developed based on the 2nd generation pi-girder that was previously tested in the laboratory. The cross-sectional parameters that were modified include girder depth, bulb width and height, web thickness, and the number of strands in the bulb. The analysis evaluated the local transverse bending capacity of the deck, the global flexural and shear capacity, and the deflection of the girder. Four cross sections with depths between 35 and 47 inches facilitating spans up to 135 feet are presented.

Keywords: Ultra-high Performance Concrete; Pi-girder; Finite element analysis; Optimization

INTRODUCTION

Ultra High Performance Concrete (UHPC) is a new generation of fiber-reinforced cementitious composite material. When compared with conventional concrete, UHPC tends to exhibit superior properties such as advanced strength, durability, and long-term stability. Previous research has derived a representative stress-strain curve of UHPC, as shown in Fig. 1 (1). Further research has focused on the compressive and tensile mechanical responses as captured from material scale tests (2,3). For the present study, the assumed UHPC uniaxial stress-strain relationship was simplified to Fig. 2, reproduced from reference 4. The tensile stress-strain relationship is elastic-perfect-plastic with an ultimate strain of 0.01 while the compressive-strain relationship is almost linear until the ultimate strength of 28 ksi (193 MPa). UHPC clearly demonstrates higher strength and better deformation capacity in tensile region than would be expected from conventional cementitious materials. It thus enables new solutions to the pressing highway bridge deterioration and congestion problems facing this sector.

The concept of using decked-girder members for bridge applications in transportation and infrastructure is not new. The double-Tee pre-tensioned concrete beam is widely used around the world in parking and other structures. In New England, governmental and industry partners are working to develop a pre-tensioned double-Tee suitable for short to medium span highway bridges. In some respects, the pi-girder investigated in this study represents an extrapolation of the double-Tee concept to engage the mechanical and durability properties of UHPC.

Advanced material properties bring about the possibility of new design solutions which heretofore may not have been possible. The advanced properties of UHPC provide opportunities for the development of new structural forms focused on addressing any number of important focus areas. The use of existing geometries for materials with advanced properties, although simple to implement, results in inefficient designs and less cost effective solutions. Therefore, it is necessary to thoroughly research to optimize the cross section for pi-girder made from UHPC.

The cross sectional dimensions of a prototype UHPC pi-girder were set through an analytical study completed at the Massachusetts Institute of Technology (5~9). Fig. 3 presents the prototype pi-girder cross section. In order to simplify girder fabrication and to address some specific structural performance concerns, modifications were necessary. The 2nd generation of pi-girder shown in Fig. 4 was developed to address these concerns. In addition to its structural efficiency, pi-section has many other advantages. For example, the pi-section is easy to inspect when compared with box girder. The slight incline surface and smooth transition in the 2nd generation pi-girder facilitate the deck drainage and make easier for bridge maintenance. It is therefore necessary to further investigate and extend this kind of section. The use of UHPC leads to a very compact strain which can accommodate space constraint in the field practice. The structural tests of 2nd generation UHPC pi-girders have been presented in reference 10. The transverse flexural capacity of the girder is sufficient and the capacity of the longitudinal joint exceeded that of the prefabricated deck. An initial

development of the UHPC pi-girder concept has been completed in Buchanan County, Iowa (11). The Jakway Park Bridge opened to traffic in late 2008. The bridge includes three adjacent 2nd generation UHPC pi-girders for two lanes of traffic.

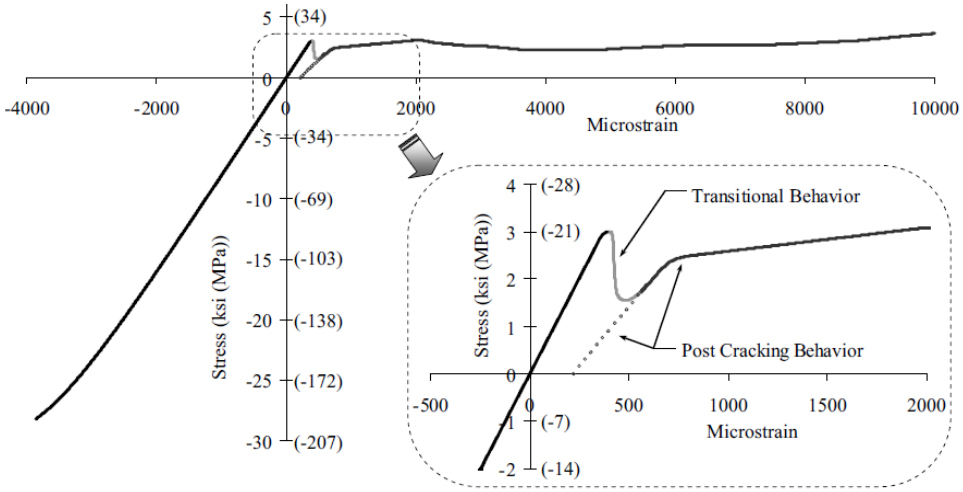

Fig. 1 Stress Strain Curve of UHPC

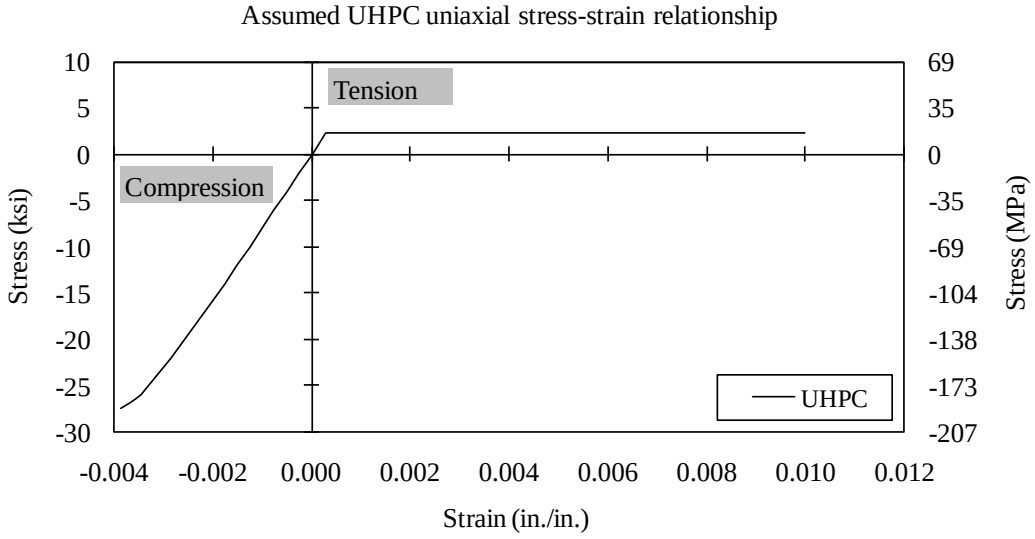

Fig. 2 Assumed UHPC uniaxial stress-strain relationship

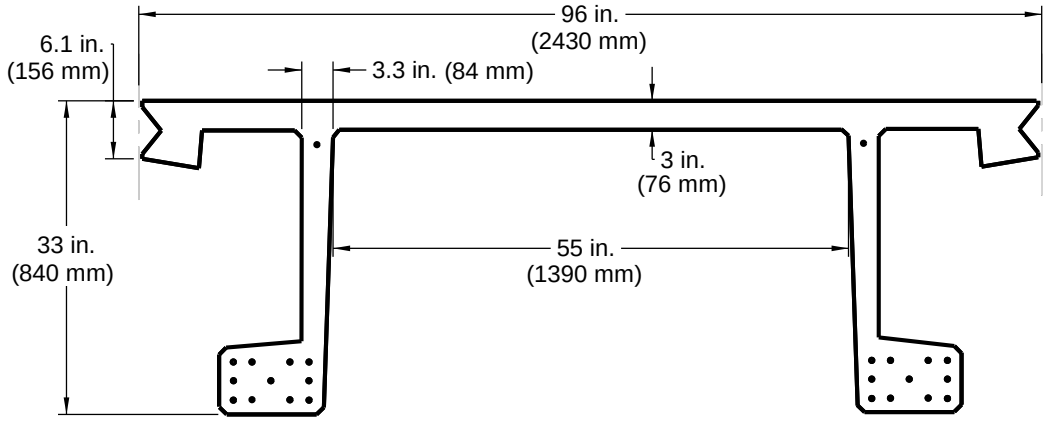

Fig. 3 Cross section for prototype UHPC pi-girder

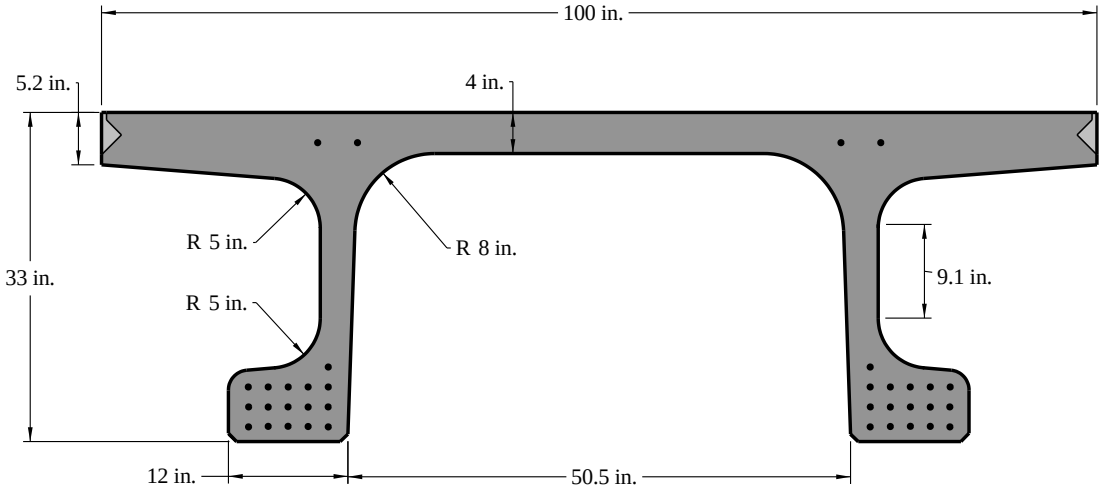

Fig. 4 Cross section 2nd generation UHPC pi-girder

Experimental study in the laboratory and field implementation has shown the feasibility of using UHPC pi-girder in the bridge design. In order to accommodate a range of different span lengths for actual bridge design, it is necessary to develop a series of cross sections. The progress in the finite element (FE) method and the advent of increasingly powerful computer provide an economic way to investigate this complex parameter analysis. The objective of this research program is to develop a series of finite element optimized sections of UHPC pi-girders using the previously calibrated finite element analysis modeling techniques. Three major factors were considered in the development of cross-sections: the transverse bending capacity of the deck in the UHPC pi-girder; the global shear and flexural capacity; the deflection under live load.

VERIFICATION OF FINITE ELEMENT ANALYSIS (FEA) MODEL

Even though the approximation of the behavior of the sections could be obtained through simplified analysis, the finite element model can provide more accurate and comprehensive insight into the performance. Finite element models emulating the structural performance of UHPC have been previously calibrated through the comparisons of five progressively more sophisticated finite element models to full-scale physical tests on flexural and shear response of a UHPC I-girder and the structural response of a 2nd generation pi-girder in reference 4,12 and 13. Once calibrated, the finite element method can also be used to conduct parameter analysis that expands the understanding of the structural behavior without physically testing the specimen. However, the finite element must have been calibrated before being utilized to conduct the analysis as the improperly modeled analysis often leads to inaccurate results.

The concrete in the finite element analysis was modeled using eight-node three-dimensional (3D) solid element. The constitutive model for the concrete used in the model is the concrete damage plasticity (CDP) model (14~17). It can handle concrete structures subjected to arbitrary loading conditions including cyclic and/or dynamic loading. It also allows stiffness recovery effects during cyclic load reversals. Density, elastic modulus, and stress-strain curve of concrete was obtained from experimental data. The 7-wire prestressing strands in the analysis were modeled using 3D solid element. In order to reduce mesh complexity in the modeled strands, the cross-section of the strands were replaced with squares of equivalent areas. The interaction between the concrete and discrete steel reinforcement such as strands was achieved by embedding the reinforcements in the concrete, assuming no bond-slip between strands and neighboring UHPC. The prestress in the strands was applied through initial conditions.

In the physical experiment, the diaphragms were used to restrain the lateral spread of the legs of pi-girder. They were simulated in the finite element model using non-linear spring elements. The axial behavior of the spring was obtained based on the actual measurements in the physical test. The boundary conditions were modeled by connecting the girder to the rigid support structure using springs. The spring in the gravity direction (Ky) was artificially assigned with very high stiffness to simulate vertical support while the stiffness for transverse springs (Kx) was assigned with very low stiffness to allow for free spreading of the pi-girder legs (as shown in Fig. 5). The model was fixed in longitudinal direction at one end. This simulated simply supported boundary conditions. The wheel pressure was applied as a distributed pressure over the contacting area of the wheels. Case specific simplifications are discussed below for each analysis.

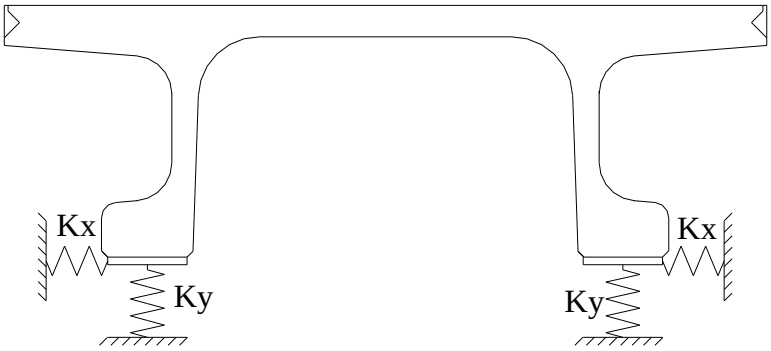

Fig. 5 Boundary conditions in finite element model

A full scale structural test was conducted in the Turner-Fairbank Highway Research Center (TFHRC) structural testing laboratory to investigate the behavior of the 2nd generation pi-girder. The girder was 33 inches (0.84 m) deep, 8.33 feet (2.54 m) wide, and can contain up to 16 prestressing strands in each bulb. The integral deck of the girder was 4.13 inches (105 mm) thick, and the webs ranged from 3.2 to 3.5 inches (81 to 89 mm) thick. A 5.25 inch (133 mm) deep shear key ran the length of each flange tip to allow for connection of the modular components. Two diaphragms were included in the test girder to assist in maintaining the integrity of the cross section during erection and under structural loading. The two diaphragms were located 6 feet (1.83m) from midspan. The measured load displacement curve for the diaphragm used was shown in Fig. 7. The girder was prestressed through the use of 0.6 inch (15.2mm) diameter, 270 ksi (1860 MPa) low-relaxation prestressing strands. The girder had 22 strands with nine in each of the two bulbs and two in the deck above each web. The strands in the bulb were all stressed to 42.5 kips (189 kN). The strands in the deck were each pulled to 5 kips (22 kN). The actual test setup was shown in Fig. 6. The girder was loaded to failure under gradually increased static loading.

Fig. 6 Test setup in the lab

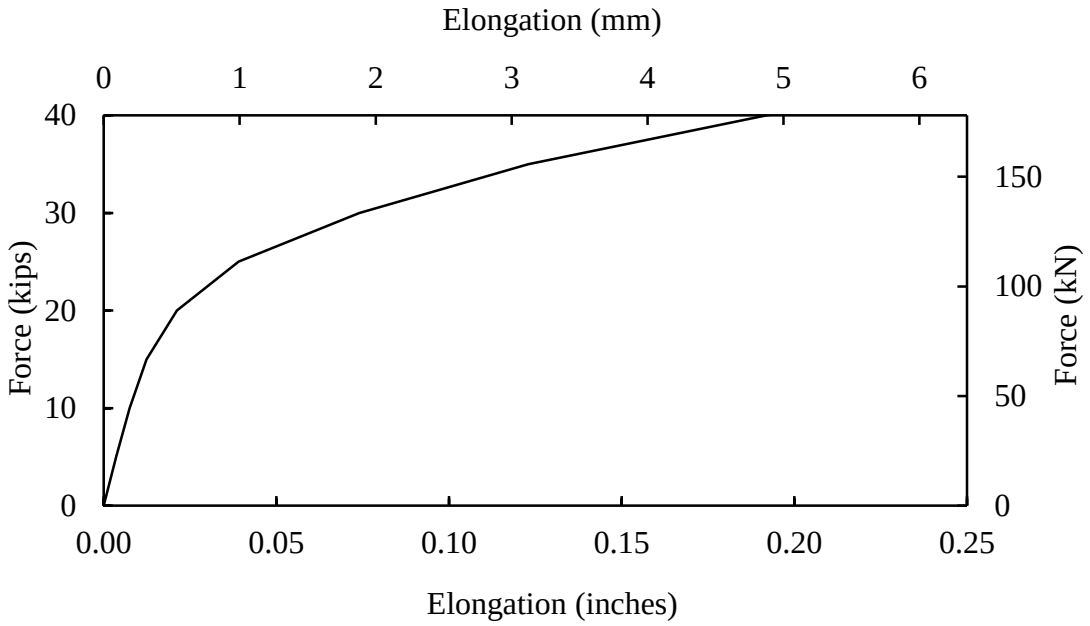

Fig. 7 Behavior of internal diaphragm

Finite element model that simulates the behavior of the girder under test was built using previously described techniques. Experimental results and results from FEA were compared in this section. Fig. 8 compares the FEA and experimentally observed vertical deflections of the bulbs at the mid-span. Fig. 9 compared the spreading of the bulb at the mid-span. Again, the experimentally observed results and the FEA results match quite well. Fig. 10 showed the difference between experimental and FEA results for the longitudinal strain at the bottom of the bulb at mid-span. Good agreements were achieved between experimental results and numerical simulation. The comparison showed that the proposed FEA model can capture the global deflection and strain distribution with reasonable accuracy. The FEA model can therefore be extended for the development of optimal cross sections for different spans.

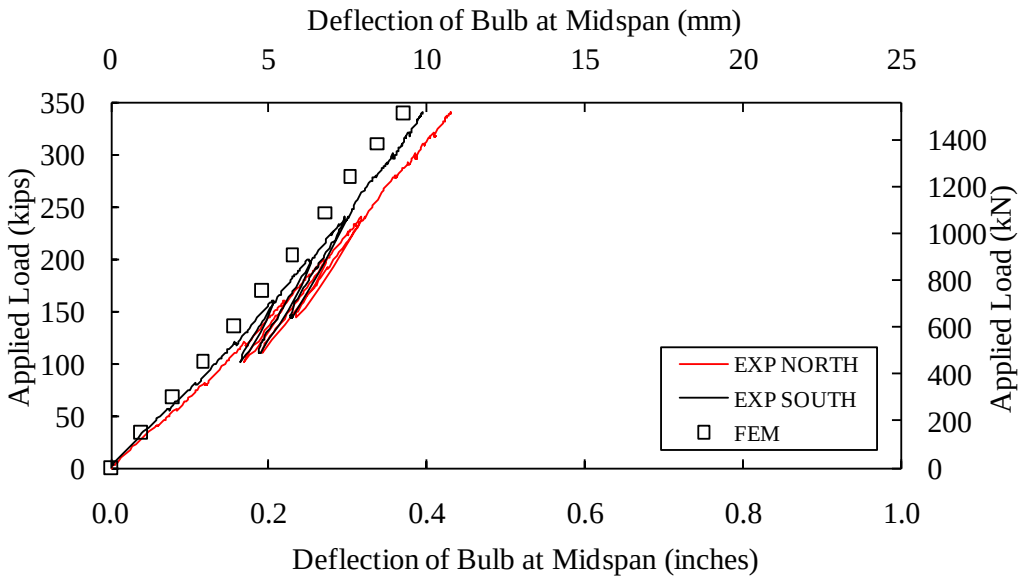

Fig. 8 Comparison of vertical bulb deflection at midspan

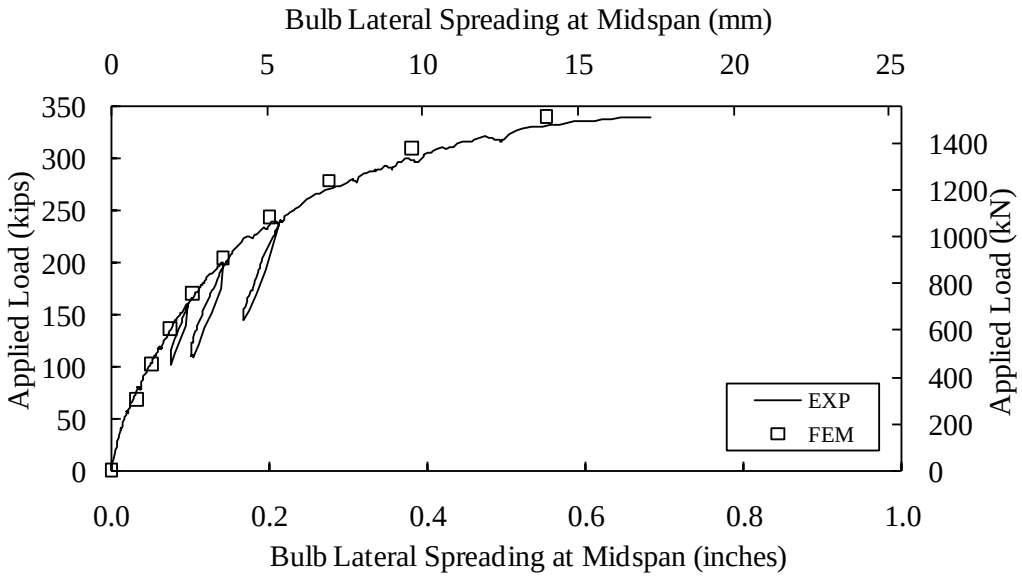

Fig. 9 Comparison of bulb spreading at midspan.

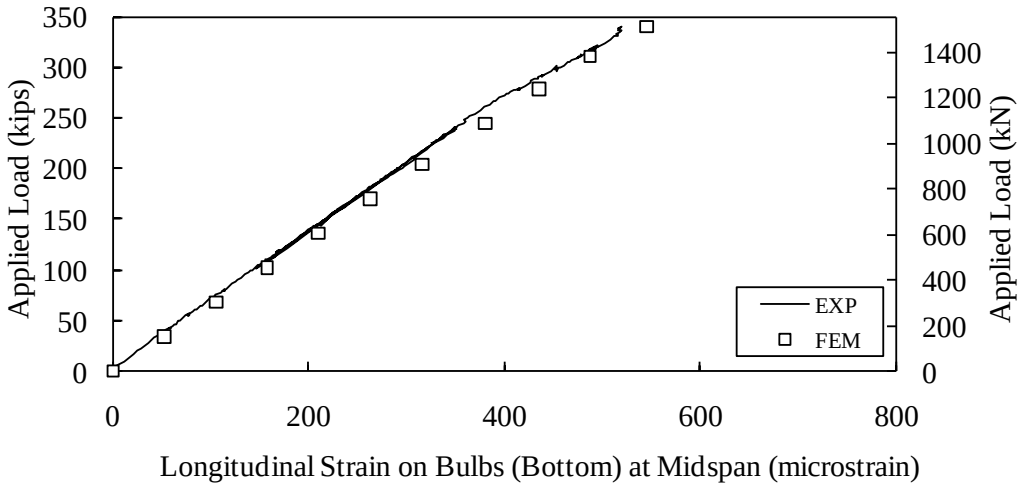

Fig. 10 Comparison of strain at bulb bottom at midspan.

DECK THICKNESS ANALYSIS

Due to the high tensile strength of the UHPC, the thickness of the deck in the pi-section can be thinner than the deck thickness of a traditional concrete bridge deck. But when the deck is too thin, the section may fail in the form of transverse bending under wheel load. The goal here becomes to find a thickness that prevents transverse bending failure of the pi-section.

The behavior of the deck in the pi-girder sections can be considered as a two-way slab. Preliminary investigation demonstrated that when the span is short, the transverse bending capacity controls the behavior of the pi-girder. This is because the web and bulb in the pi-section stiffen the section in the longitudinal direction as compared with the transverse direction. When the span length increases, the flexural capacity in the longitudinal direction is relative weaker compared with the flexural capacity in transverse direction. In order to investigate the transverse bending capacity, it is important that other failure modes such as longitudinal flexural failure and shear failure be suppressed. Therefore, a short span model is needed to suppress the longitudinal failure and investigate the transverse bending capacity. In this portion of the research the span length used in the deck thickness analysis is 15 feet (4.57 m), which is close to diaphragm spacing used in the Jakway Park Bridge (11). Diaphragm stiffness plays an important role on the transverse behavior. In this section, three different stiffness values were considered: stiff diaphragms, regular diaphragms and soft diaphragms. The stiffness for the regular diaphragm was obtained from the physical tests. The stiffness behavior was shown in Fig. 7. The stiffness of the stiff diaphragm was artificially assigned with a high value while that of the soft diaphragms were assigned with a very small stiffness. Stiffness for stiff and soft diaphragms were $1X10^{15}$ lb/in. (or $1.75X10^{17}$ N/m) and $1X10^{-8}$ lb/in. (or $1.75X10^{-6}$ N/m), respectively.

Since the span of the model is only 15 feet (4.57 m), only one wheel load was applied in the longitudinal direction (i.e., in the traffic direction) on the model. Considering the multiple lanes that may be present on a bridge, it is possible that two trucks may pass through the bridge side by side. Therefore, the wheel load in this section was modeled as two wheel patches adjacent to each other. This is unrealistic but conservative. For one reason, two trucks cannot drive side by side with tires touching each other; for another, the load distribution of adjacent girder was not considered. Fig. 11 shows the finite element model for the deck thickness analysis.

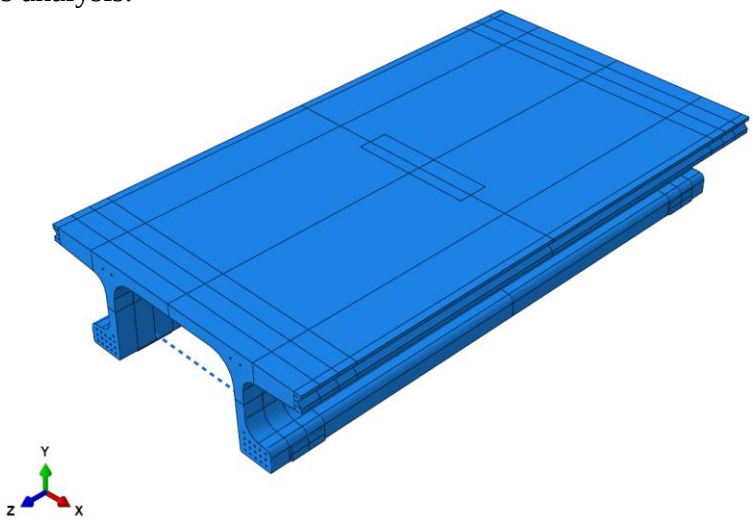

Fig. 11 Finite element model for deck thickness analysis

Table 1 summarizes the maximum tensile strain at midspan under the AASHTO LRFD Strength I load condition. The value in the table is obtained through linear interpolation using results from two closest time steps when the load applied in these steps is not exactly the standard Strength I load according to AASHTO LRFD. For example, if the strain was 176 με when the load is 91.25% of the Strength I load and became 401 με when the load is 141.2% of the Strength I load, the strain under 100% Strength I load was determined to be 207 με according to linear interpolation. All three candidate deck thickness can sustain the loading without exceeding the limit on the maximum tensile strain (3000 με). The stiffness of the diaphragms have a significant effect on the transverse bending behavior. The principal strain reduces greatly when a regular diaphragm was added. The diaphragm stiffness has a greater impact on the principal tensile strain for thinner decks. More details can be found in the final report for this project (18).

Table 1. Maximum principal strain (με) at the midspan under Strength I load case.

Deck Thickness (inch (mm))	Maximum Principal Strain (με)		
	Stiff Diaphragm	Regular Diaphragm	Soft Diaphragm
4.5 (114)	149	152	252
4.0 (102)	182	191	363
3.5 (89)	196	207	756

Table 2 listed the results of maximum wheel load for different deck thicknesses when the maximum tensile strain limit is reached. The load ratio in the table is defined as the ratio between the maximum wheel load and the AASHTO LRFD wheel load. The failure criterion was reached when the principal tensile strain in the concrete reaches 3000 με. The criterion also applies to the strength analysis described in the next section. The value in the table is obtained through linear interpolation using results from two closest time steps when the maximum principal strain in the results is not exactly 3000 με. The results show that the introduction of the diaphragm increases the maximum wheel load significantly. The beneficial effect of the diaphragms was more significant in the models with a thinner deck (3.5 inches (89 mm)) than for models with a thicker deck (4.5 inches (114 mm)). All candidate thicknesses for the deck can sustain the requirement of AASHTO LRFD wheel load with a load ratio greater than 1.0. For a 4-inch (102 mm) deck with 15 feet (4.57 m) diaphragm spacing, the load ratio is 3.840. This indicates that the deck can sustain a wheel load 3.84 times the standard AASHTO wheel load, corresponding to a wheel load 61.44 kips (251 kN) of over a patch area of 20"X10" (51mmX25mm). Based on these results and practical construction considerations, the 4.0 inch (102 mm) thick deck was selected for use throughout the remainder of the study.

FLEXURE AND SHEAR CAPACITY

To facilitate preliminary design for bridge designers, it is desirable to develop different cross sections for different span length. This section focuses on the development of different sections that satisfy global flexural and shear strength (under Strength I limit state in AASHTO) for different span lengths. To facilitate the efficient use of formwork, it is necessary to keep the slope of certain surfaces and fillet radii unchanged for all cross-sections in the development of the new cross sections. The surfaces whose slopes are kept constant are noted in Fig. 12. The increment for girder height was determined to be 4 inches () and the increment in the bulb size (height and width) was 2 inches () in this research. In this way, a standard set of formwork with included filler pieces can allow for the fabrication of multiple girder cross sections.

A single girder model was used to investigate the relationship between cross section parameters and the span length. Since this section focuses on the global behavior, the local failure mode should be prevented. The wheel load was applied above the web to suppress transverse bending failure. The magnitude of the load corresponds to the standard AASHTO Strength I wheel load. In the investigation of flexure capacity, the design truck was simulated by applying the entire load of the design truck on the wheel patch at midspan. Again, this is unrealistic but more conservative. In the analysis of global shear behavior, the load was applied at a distance of three times the girder depth away from the support point in order to create a maximum shear response in the web. Fig. 13 shows a typical FE model for the global strength analysis.

After trial and error, four cross sections were developed for different spans as shown in Fig. 14 to Fig. 17. More detailed results were summarized in Table 3. In the table, the strand layout was named by the number of strands in each row starting from the bottom. For

example, layout "6-6-6-6-2" means there are five layers of strands in the bulb. The first four layers from the bottom have 6 strands and the fifth layer from the bottom has 2 strands. It should also be noted that the stress and strain results in this section result from the combined effect from prestress, dead loads and live loads. It can be seen that the proposed cross sections can be used for span of up to 135 feet (41.1m). It can also be seen that except for Section I, sections for larger span do not have full strand layout, indicating that the cross section is controlled by other factors, such as the deflection under life load discussed in the next section.

Table 2. Maximum load ratio when the strength limit state is reached.

Deck Thickness (inch (mm))	Load Ratio		
	Stiff Diaphragm	Regular Diaphragm	Soft Diaphragm
4.5 (114)	5.228	4.456	2.251
4.0 (102)	4.300	3.840	1.748
3.5 (89)	3.428	3.204	1.222

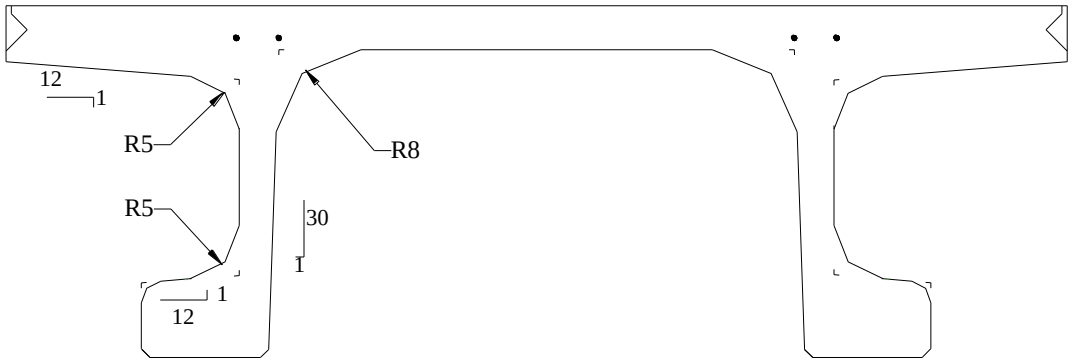

Fig. 12 Unchanged parameters for cross section series

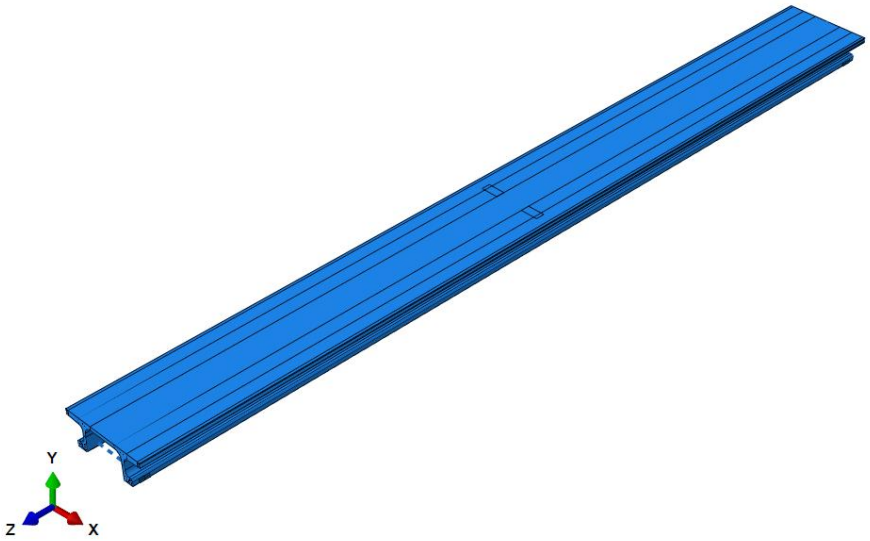

Fig. 13 Typical Finite Element Model for Global Flexure Analysis

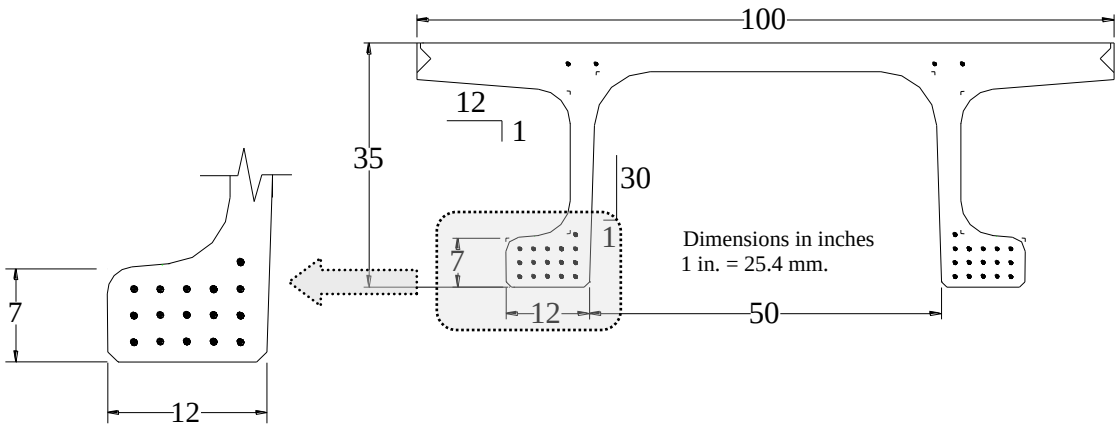

Fig. 14 Strand layout of 35-inch-deep section for 80-foot (24.4m) span

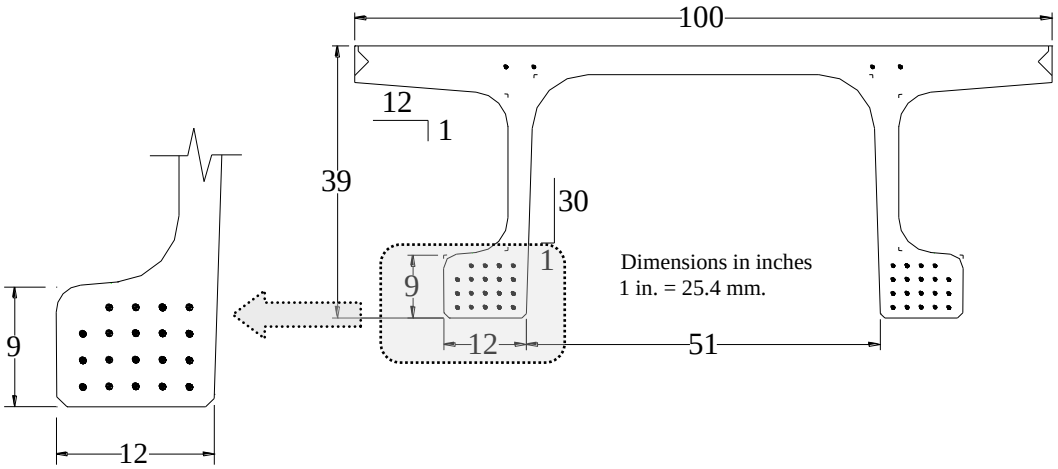

Fig. 15 Strand layout of 39-inch-deep section for 95-foot (29.0 m) span

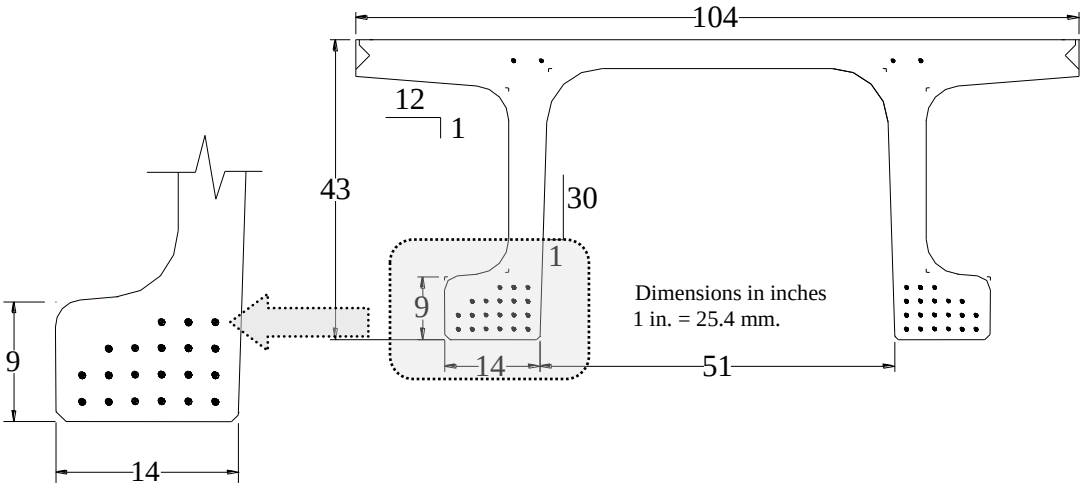

Fig. 16 Strand layout of 43-inch-deep section for 105-foot (32.0m) span

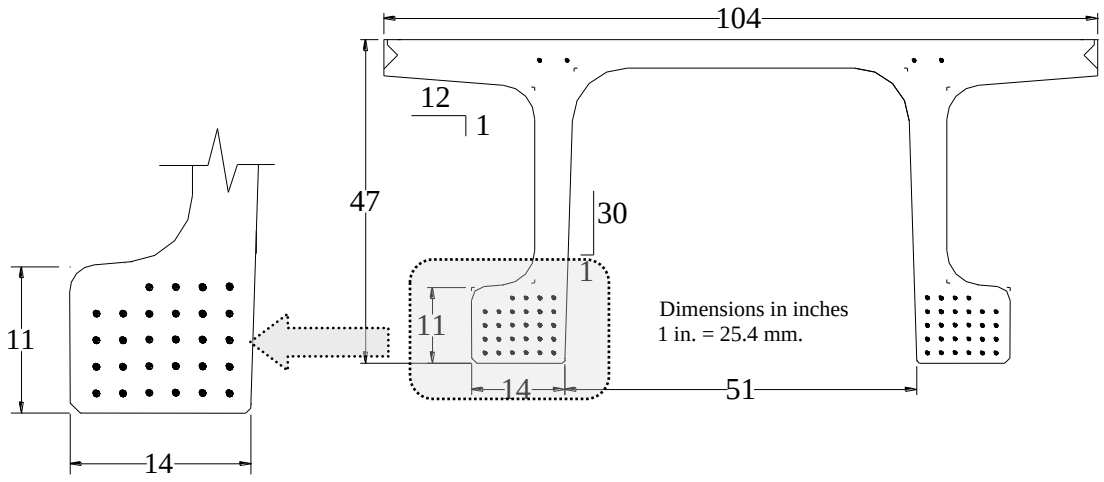

Fig. 17 Strand layout of 47-inch-deep section for 135-foot (41.1 m) span

Table 3. Refined cross sections for different span length.

Section ID	Section I	Section II	Section III	Section IV
Span (feet (m))	80 (24.4)	95 (29.0)	105 (32.0)	135 (41.1)
Girder depth (inch (mm))	35 (889)	39 (991)	43 (1092)	47 (1194)
Deck Width (inch (mm))	100 (2540)	100 (2540)	104 (2642)	104 (2642)
Web Thickness (inch (mm))	3.37 (85.6)	3.33 (84.5)	5.27 (133.8)	5.23 (132.8)
Bulb Width (inch (mm))	12.03 (305.6)	11.90 (302.3)	13.77 (349.8)	13.63 (346.2)
Bulb Height (inch (mm))	7.25 (184.2)	9.25 (235.0)	9.16 (232.7)	11.25 (285.8)
Strand layout	5-5-5-1	5-5-5-4	6-6-5-3	6-6-6-6-4
Flexure: Max Tensile Strain at Midspan (με)	2826	2531	2520	2694
Flexure: Max Longitudinal Stress in Strands (ksi (MPa))	251 (1730)	247 (1703)	248 (1710)	250 (1724)
Shear: Max Tensile Strain in the Web (με)	457	291	159	189

DEFLECTION ANALYSIS

In addition to the strength limit state, AASHTO LRFD also contains language regarding the flexibility of the structure under live load. The deflection should be taken as the larger of the deflection due to design truck alone or due to 25% of the design truck together with the design lane load. The impact factor should be considered when calculating the wheel loads. The requirement on the deflection should be limited to 1/800 of the span length. This section checks whether the deflection of the proposed sections can meet the requirement specified in AASHTO.

In this section, a 3-girder bridge model was used. The deck widths of the developed cross sections are 100 inches (2540 mm) or 104 inches (2591 mm). A three-girder system is enough to accommodate two traffic lanes. It is conservative compared with other combinations of girder numbers and lane numbers. For simplicity, the interface between adjacent girders in the 3-girder model was assumed to be perfectly bonded, i.e., no slip occurs at the interface. The magnitude for traffic load was defined in AASHTO LRFD, but the location or pattern of the applied load also have influence on the deflection. Compared with interior girder, the exterior girder usually has greater deformation under the same load because only one girder can help distribute the load. Fig. 18 shows the relative location of the wheel load and lane load. This load pattern creates maximum possible deflection at the exterior web/leg in the exterior girder and the exterior girder. In this section, a diaphragm spacing of 15 feet (4.57 m) was used. This diaphragm spacing was selected based on previous experience in the field (11). There are two types of diaphragms in the model for deflection check. The inter-diaphragm is the diaphragm that connects the two “legs” within the same pi-girder piece and the intra-diaphragm refers to the diaphragm that connects the adjacent girders. The inter- and intra- diaphragms were placed at the same location along the longitudinal direction of the girder. The stiffness of the inter-diaphragm was the same as those used in previous analysis. The stiffness of the intra-diaphragm was calculated based on the length of the diaphragm using the equation for springs in series.

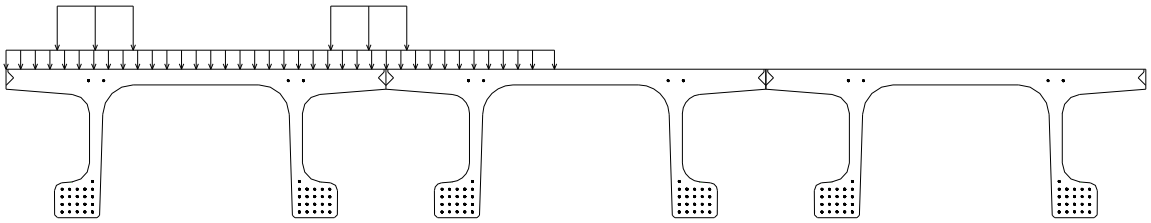

Fig. 18 Load pattern for live load deflection check

Trial simulation indicates that the deflection was controlled by the truck load only for all cases. Therefore only the deflection under truck load was checked in this section. Table 4 summarizes the flexural strain and deflection check for the refined cross-sections. Combining the results of this section and previous section, it can be seen that strain under Strength I load for all cross sections are less than 3000 με and the deflection under live load is less than the 0.125% of the span length. Therefore, all the proposed cross sections passed the strength and deflection check.

Table 4. Deflection under truck loads for refined cross sections.

Section ID	Section I	Section II	Section III	Section IV
Span (feet (m))	80 (24.4)	95 (29.0)	105 (32.0)	135 (41.1)
Midspan Deflection (inch (mm))	1.13 (28.7)	1.35 (34.3)	1.51 (38.4)	1.98 (50.3)
Deflection/Span (%)	0.118	0.118	0.120	0.122

MODIFIED CROSS SECTIONS FOR SHORTER SPANS

In practice, the bridge span may be shorter or longer than the target span evaluated in the previous sections. To facilitate use of these results, it is necessary to investigate the possible span range for each type of cross sections. The span lengths in the previous sections were the maximum possible span for each cross section. The applicability of cross sections on smaller spans needs to be studied. To achieve this, a parametric analysis was conducted to find the maximum span for sections with the same depth but different strand layouts. It is possible that the strands be eliminated by using a deep cross section on a short span. However, this may not be economically appropriate. In this research, only a limited span range was investigated for each section. Since each section was applied on a shorter span, the deflection requirement was automatically met. The shear capacity was also not checked in this section as the shear load was unchanged. The single bridge model similar to those for global flexural analysis under Strength I load was used in this section. The results of using the section with fewer strands on small span were summarized in Table 5. The nomenclature of the strands was the same as defined in previous sections. Combining results from previous sections, Fig. 19 shows a graphic representation of the applicable span range for each girder depth.

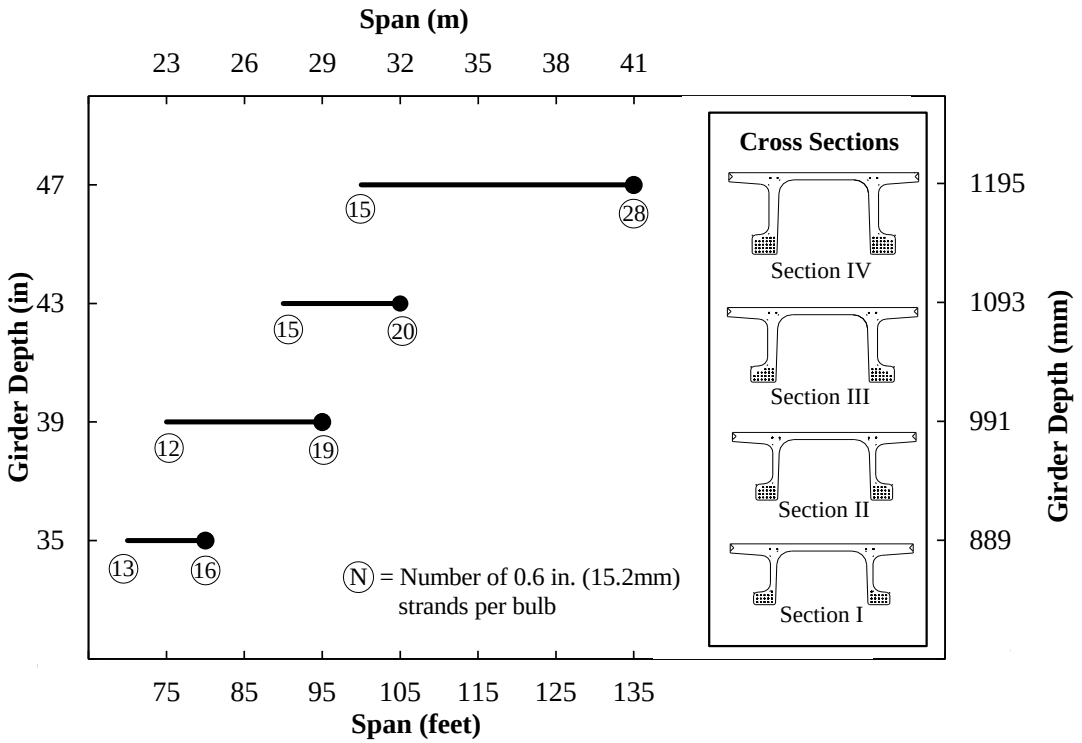

Fig. 19 Design chart for proposed sections

Table 5. Modified cross sections for application on smaller span length.

Section ID	Section I	Section II	Section III	Section IV
Span (feet (m))	70 (21.3)	75 (22.9)	80 (24.4)	100 (30.5)
Girder depth (inch (mm))	35 (889)	39 (991)	43 (1092)	47 (1194)
Deck Width (inch (mm))	100 (2540)	100 (2540)	104 (2642)	104 (2642)
Web Thickness (inch (mm))	3.37 (85.6)	3.33 (84.5)	5.27 (133.8)	5.23 (132.8)
Bulb Width (inch (mm))	12.03 (305.6)	11.90 (302.3)	13.77 (349.8)	13.63 (346.2)
Bulb Height (inch (mm))	7.25 (184.2)	9.25 (235.0)	9.16 (232.7)	11.25 (285.8)
Strand layout	5-5-3	5-5-2	6-6-3	6-6-3
Max Flexural Strain at Midspan (με)	2301	2326	2273	2285
Max Longitudinal Stress in Strands (ksi (Mpa))	244.0 (1862)	244.1 (1863)	243.8 (1681)	243.7 (1680)

CONCLUSIONS

The following conclusions are presented based on the research presented in this report.

1. The behavior of the UHPC can be appropriately modeled through the use of the existing concrete damage plasticity model within the finite element software package. The finite element model was capable of re-producing load-displacement curve and strain distribution with reasonable accuracy and therefore considered valid for further analysis.

2. The results from the parameter analysis on the deck thickness showed that the stiffness of the diaphragm impacts the transverse bending capacity of the pi-girders. Even though a deck thickness of 3.5 inches (89 mm) was sufficient to resist standard AASHTO load (Strength I), a deck thickness of 4 inches (102 mm) is recommended considering construction tolerances and convenience in re-using existing formwork.

3. A family of UHPC pi-girders was developed for spans ranging up to 135 feet (41.1 m). These decked girders, with depths of 47 inches (1194 mm) or less, were designed to resist loads in excess of those required by the AASHTO LRFD Bridge Design Specifications while meeting the live load deflection recommendations.

4. The proposed sections can be applied on shorter spans by reducing the number of prestress strands in the bulb. A design chart was provided based on the parameter analysis using finite element method. The chart can facilitate the selection of cross sections in the preliminary design stage.

ACKNOWLEDGEMENTS

The publication of this article does not necessarily indicate approval or endorsement of the findings, opinions, conclusions, or recommendations either inferred or specifically expressed herein by FHWA or the United States Government.

The research discussed herein was conducted by Professional Service Industries, Inc. at the FHWA Turner-Fairbank Highway Research Center under laboratory support contract DTFH61-10-D-00017.

REFERENCES

1. Graybeal, B., “Structural Behavior of Ultra-High Performance Concrete Prestressed I-Girders,” Federal Highway Administration, Report No. FHWA-HRT-06-115, August 2006, 104 pp.
2. Graybeal, B., “Compressive Behavior of Ultra-High Performance Fiber-Reinforced Concrete,” ACI Materials Journal, V. 104, No. 2, March-April 2007, pp. 146-152.

3. Graybeal, B., and Baby, F., "Development of a Direct Tension Test Method for Ultra-High-Performance Fiber-Reinforced Concrete," ACI Materials Journal, V. 110, No. 2. March-April 2013, pp. 177-186.
4. Chen, L., and Graybeal, B., "Finite Element Analysis of Ultra-High Performance Concrete: Modeling Structural Performance of an AASHTO Type II Girder and a 2nd Generation Pi-Girders," Federal Highway Administration, NTIS Accession No. PB2011-100864, October 2010, 177 pp.
5. Chuang, E., and F. Ulm, "Two-Phase Composite Model for High Performance Cementitious Composites," Journal of Engineering Mechanics, V. 128, No. 12, 2002, pp. 1314-1323.
6. Chuang, E., "Ductility Enhancement of High Performance Cementitious Composites and Structures," Massachusetts Institute of Technology, 2002, 319 pp.
7. Soh, M., "Model-Based Design of a Ultra High Performance Concrete Prototype Highway Bridge Girder," Massachusetts Institute of Technology, 2003, 64 pp.
8. Park, H., "Model-Based Optimization of Ultra High Performance Concrete Highway Bridge Girders," Massachusetts Institute of Technology, 2003, 139 pp.
9. Graybeal, B., "Structural Behavior of a Prototype Ultra-High Performance Concrete Pi-Girder," Federal Highway Administration, NTIS Accession No. PB2009-115495, 2009, 145 pp.
10. Graybeal, B., "Structural Behavior of a 2nd Generation Ultra-High Performance Concrete Pi-Girder," Federal Highway Administration, NTIS Accession No. PB2009-115496, 2009, 102 pp.
11. Graybeal, B., "UHPC making strides", Public Roads, 72 (4), 17pp.
12. Chen, L., and Graybeal, B., "Modeling Structural Performance of Ultra-High Performance Concrete I-Girders," ASCE Journal of Bridge Engineering. V. 17, No. 5, September-October 2012, pp. 754-764.
13. Chen, L., and Graybeal, B., "Modeling Structural Performance of 2nd Generation Ultra-High Performance Concrete Pi-Girders," ASCE Journal of Bridge Engineering. V. 17, No. 4, July-August 2012, pp. 634-643.
14. Chen, W. F., "Plasticity in Reinforced Concrete," McGraw-Hill, Inc., 1982, 474 pp.
15. Hillerborg, A. M. Modeer, and P. E. Petersson, "Analysis of Crack Formation and Crack Growth in Concrete by Means of Fracture Mechanics and Finite Elements," Cement and Concrete Research, V. 6, 1976, pp. 773-782.
16. Lee, J., and G.L. Fenves, "Plastic-Damage Model for Cyclic Loading of Concrete Structures," Journal of Engineering Mechanics, V. 124, No.8, 1998, pp. 892–900.
17. Lubliner, J., J. Oliver, S. Oller, and E. Oñate, "A Plastic-Damage Model for Concrete," International Journal of Solids and Structures, V. 25, No.3, 1989, pp. 229–326.
18. Zhang, G, Graybeal, B. and Chen, L., "Development of a Family of Ultra-High Performance Concrete Pi-Girders", Federal Highway Administration Report (In Press)